analytical chemistry

pubs.acs.org/ac Article

DNAzyme-Powered DNA Walker for Cooperative Expression Imaging of Mutant p53 and Telomerase in Cancer Cells

Ze-Rui Zhou, Da-Wei Li, Ruo-Can Qian,* and Huangxian Ju*

Cite This: *Anal. Chem.* 2023, 95, 4122−4130 Read Online

ACCESS | Metrics & More | Article Recommendations | Supporting Information

ABSTRACT: Cooperative expression of multiple cancer biomarkers is of great significance in influencing cell pathways and drug treatment. However, the simultaneous analysis of low-abundance biomarkers in living cells remains a challenge. Here, we report a DNAzyme-powered DNA walker to visualize the cooperative expression of mutant p53 and telomerase in living cells. The activation of the DNA walker is orthogonally powered by mutated p53 and telomerase, which enables the unlocking of the walking strand and the subsequently repeated substrate cleavage, producing fluorescence recovery for the imaging of the two target molecules in living cells. The DNA walker allows for real-time monitoring of the expression profile of mutant p53 and active telomerase in cancer cells under various antitumor drug treatments, and the results demonstrate the cooperative expression of mutant p53 and telomerase via the Akt pathway, which may bring new insights into the study of cancer pathway-relevant biomarkers.

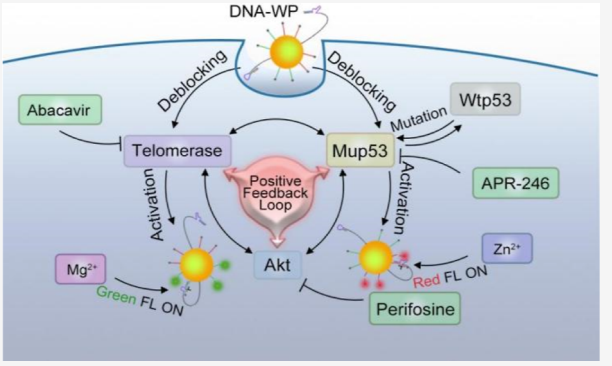

INTRODUCTION

Cancer is a leading cause of death worldwide, which specifies a cluster of diseases affecting almost each part of the body.[1,2] It is of great significance to visualize and detect intracellular cancer-related molecules for the research of cancer pathophysiology, diagnosis, and therapy. However, the abundance of some important intracellular cancer biomarkers, especially cell survival regulatory proteins, is extremely low, leading to the difficulty in detection. What is more, it is more difficult to determine possible cooperative expression of different biomarkers, although it has shown an important influence on cell pathways and drug treatment. Thus, it is desirable to develop an effective one-to-more signal amplification strategy for sensitive detection and imaging of multiple low-abundance cancer biomarkers in living cells, revealing the interconnections and possible cross talks among different cellular pathways.[3]

In this study, we choose p53 and telomerase as the targets to develop a customizable detection strategy for intracellular imaging of their cooperative expression. P53 is a tumor suppressor protein related to the regulation of the cell cycle and programmed cell apoptosis.[4,5] The central part in this process is the binding of tetrameric p53 to regulatory DNA motifs in the genome of the 20-bp consensus double strand.[6,7] P53 mutations in cancer often lead to the inactivation of its DNA binding domain, as mutant p53 not only loses its tumor suppressor activity but also induces carcinogenesis that gives cancer cells a growth advantage over normal cells.[8,9] The abnormal expression of mutant p53 has been regarded as an important marker of tumorigenesis. Telomerase is a specialized RNA-directed DNA polymerase that can extend telomeres of eukaryotic chromosomes for maintaining genomic stability and cell viability.[10] Due to its high expression in most human cancers,[11,12] it is also considered as an important diagnostic and prognostic cancer biomarker.[13] In particular, both p53 and telomerase are closely linked with cancer cell survival and tumor progression. Therefore, it is important to evaluate p53 mutation and telomerase activation simultaneously.

Various procedures have been applied to detect p53 or telomerase, including traditional methods like enzyme-linked immunosorbent assay (ELISA), electrochemical methods, mass spectrometry, and radioimmunoassay.[14−19] Some sensitive p53 or telomerase biosensors with a simple design and operational ease have also been constructed with electrochemical, optical, and mass-sensitive strategies.[20−23] Although these methods are highly sensitive and convenient, most of them are focused on the determination of p53 or telomerase individually in cell lysates or tissue samples, thus unable to provide the spatiotemporal distribution of targets in living cells. Therefore, it is highly desirable to develop in situ imaging strategies for detecting intracellular p53 and telomerase, especially the expression of mutant p53 and active telomerase in living cells, which may provide valuable information to

Received: November 15, 2022
Accepted: February 9, 2023
Published: February 17, 2023

https://doi.org/10.1021/acs.analchem.2c05111
Anal. Chem. 2023, 95, 4122−4130

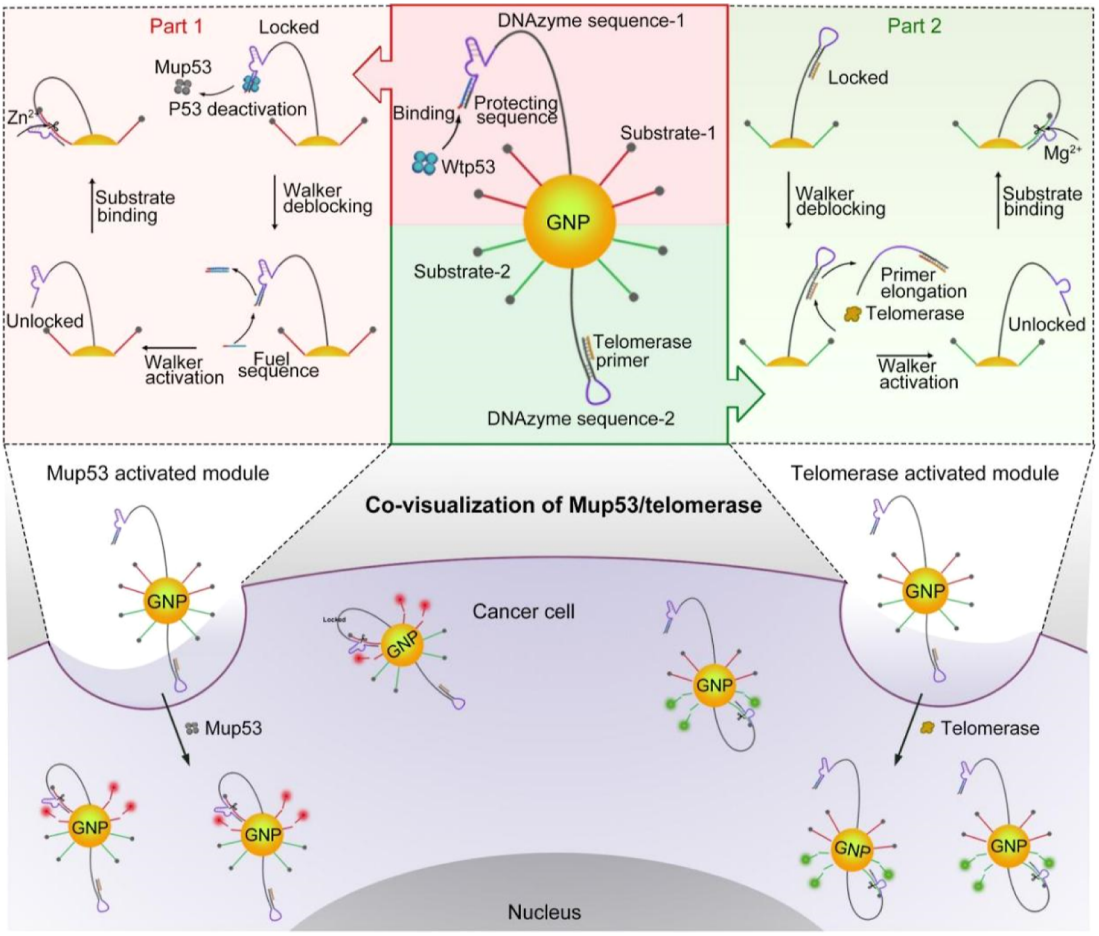

Figure 1. Schematic illustration of the DNAzyme-powered DNA walker. Top: working principle of the fuel sequence-triggered, DNAzyme-powered fluorescence activation and amplification for the detection of mup53 (Part 1) and telomerase (Part 2). Bottom: fluorescence imaging of mup53 and telomerase in living cancer cells.

understand the interconnections between the activation of telomerase and p53 mutation in cellular pathways involved in carcinogenesis and the therapeutic outcome.

Recently, synthetic molecular machines that perform quasi-mechanical movement at the micro−nano-scale under appropriate external stimuli have attracted significant attention, owing to their self-directed movement and excellent signal amplification capability.[24−26] Among these artificial molecular machines, DNA walkers are especially attractive due to the precise base pairing of DNA strands, DNA sequence programmability, structural controllability, good biocompatibility, facile synthesis, and easy modification.[27−31] With the combination of the fluorescence dyes and confocal microscopes, DNA walkers have been successfully applied in biosensing and cell imaging.[32−34] As typical building blocks of DNA walkers, DNAzymes are a class of catalytic DNA molecules that can perform an enzymatic function triggered by specific metal ions.[35−38] The susceptibility of DNAzymes to metal-dependent cleavage can effectively manipulate the breakage of ribonucleotides, enabling the manipulation of mechanical movement.[33] Inspired by the unique mechanical properties of DNAzymes, here we employ metal ion-specific RNA-cleaving DNAzymes and their respective substrate strands to build a DNAzyme-powered DNA walker for sensitive visualization of low-abundance mutant p53 and telomerase in living cells (Figure 1).

The designed DNA walker is constructed by assembling Zn^{2+}-dependent DNAzyme walking strands, Mg^{2+}-dependent DNAzyme walking strands, fluorescent dye-labeled substrate strands, protecting sequence, fuel sequence, and telomerase primer (TSP) on the surface of a gold nanoparticle (GNP). The walking strand contains a DNAzyme sequence in the middle, with its 3′-end locked by the protecting sequence or TSP to deactivate the DNAzyme. The fluorescence of substrate strands is quenched by the GNP core. After entering cancer cells, the DNAzyme walking strands can be orthogonally unlocked by the target biomarkers, thus inducing the subsequently repeated cleavage of the substrates to turn on the fluorescence. In this process, the DNAzyme activity can be recovered by a trace amount of mutant p53 or telomerase, thus greatly enhancing the detection sensitivity. This strategy is capable of imaging mutant p53 and telomerase in a single living cell, showing great potential in clinical diagnosis and cancer research.

EXPERIMENTAL SECTION

Materials and Reagents. HeLa cervical cancer cells, MCF-7 cells, and LO2 cells were purchased from bluefbio (Shanghai) Biology Technology Development Co., Ltd. (Shanghai, China). The CCK-8 kit was obtained from Thermo Fisher Scientific Inc (Waltham, MA, USA). $ZnCl_2$ and $MgCl_2$ were purchased from Adamas-beta (Shanghai, China).

https://doi.org/10.1021/acs.analchem.2c05111
Anal. Chem. 2023, 95, 4122−4130

Chloroauric acid ($HAuCl_4{\cdot}4H_2O$), sodium borohydride, and trisodium citrate were obtained from Sinopharm Chemical Reagent Co., Ltd. (Beijing, China). Anti-mup53/FITC, anti-TERT/CY5, and anti-Akt/AF350 were obtained from Beijing Bioss Biotechnology Co., Ltd. (Beijing, China). Phosphate buffer saline (pH 7.4, PBS) contained 136.7 mM NaCl, 2.7 mM KCl, 8.72 mM Na_2HPO_4, and 1.41 mM KH_2PO_4. Aqua regia was prepared by mixing HCl and HNO_3 with a volume ratio of 3:1. All aqueous solutions were prepared using ultrapure water (≥18 MΩ·cm, Milli-Q, Millipore). All DNA sequences were purchased from Sangon Biological Engineering Technology Co., Ltd. (Shanghai, China), and the characterization of these sequences is provided in Figure S1 and S2. To prepare the super hairpin secondary structure, DNA strands were snap-cooled in TE buffer supplemented according to the reported protocol (heated at 94 °C for 5 min and put at room temperature for 1 h before use). The DNA and RNA sequences are given below (from 5′ end to 3′ end).

Walking strand-1: HS-T(40) ATA GTT TCT CCG AGC CGG TCG AAA CTT CTC TAC CTG CAA GGG CAT GTC TGG GCA TGT CT.

Protecting sequence: TTT TTA GAC ATG CCC AGA CAT GCC CTT GCA G.

Fuel sequence: CTG CAA GGG CAT GTC TGG GCA TGT CTA AAA A.

Substrate-1: HS-T(10) TTG CAG GTA GAG AAG T/rA*/G GAA ACT AT-TAMRA.

Walking strand-2: HS-T(40) AGG GTT GTT GAC CGA AGG CTA GCT ACA ACG ACT TCC ATG ACA ACC CTA ACT CTG CTC GAC GGA TT.

TSP: AAT CCG TCG AGC AGA GTT.

Substrate-2: HS-U(10) GGU GGU CAU GGA AGG* U*UC GGU CAA CGG CCA-FAM.

The DNA base marked with "*" is the cleavage site for metal ions.

Apparatus. All the fluorescence images were obtained using a water-dipping objective (60×) on a laser scanning confocal microscope (Nikon A1R., Japan). All materials were weighed by an analytical balance (ME 104, METTLER TOLEDO), and all reagents were centrifuged by a centrifuge (Centrifuge 5430, Eppendorf). The fluorescence spectra were gained on an FL spectrophotometer (LS-55 Lumine). Transmission electron microscopy (TEM) (JEOL Ltd., Japan) was used to describe the morphology of AuNPs and DNA-walker probe (DNA-WP). UV−vis absorption spectra (Ocean Optics Inc., USA) were utilized to characterize the assembled process of the DNA-WP. Dynamic light scattering (DLS) experiment was conducted on a 90 Plus/BI-MAS equipment (Brook Haven).

Cell Culture and Extraction of Telomerase and mup53. HeLa cells and MCF-7 cells were cultured in DMEM with 1% penicillin/streptomycin and 10% FBS. LO2 cells were cultured in RPMI-1640 with 1% penicillin/streptomycin and 10% FBS. All cells were cultured in a humidified atmosphere containing 5% CO_2 at 37 °C. HeLa cells were collected in an Eppendorf (EP) tube and washed twice with ice-cold PBS solution (pH 7.4). The collected cells were lightly mixed in 200 μL of CHAPS lysis buffer for 30 min. Then, the mixture was centrifuged (13,000 rpm, 20 min) at 4 °C. Subsequently, the supernatant was shifted to a new RNase-free EP tube and immediately used for detection or frozen at −80 °C.

Preparation of the DNA-WP. 15 nm AuNPs were prepared according to the classical sodium citrate reduction method. Briefly, 100.0 mL of $HAuCl_4$ (0.01%, w/v) solution was boiled under mighty stirring. Then, 2.5 mL of trisodium citrate aqueous solution (1%, w/v) was added to the solution under vigorous stirring. After the solution color changed to deep red, the reaction was stopped. Finally, the cooled solution of AuNPs was stored at 4 °C. In addition, all hairpin probes were prepared by mixing the DNAzyme sequence and protecting sequence (or primer elongation) at a molar ratio of 1:2 along with the annealing process for further use. To construct a DNAzyme-powered DNA-WP, the hairpin probes and substrates were thiolated to bind to the AuNPs by the Au−S bond. In brief, 10 μL of hairpin probes (10 μM) and 50 μL of substrates (20 μM) were added to 600 μL of AuNP (10 nM) suspension and stirred at 25 °C for 24 h. Under stirring, 100 μL of NaCl (1 M) was stepwise added to the mixture solutions to load more DNA. To get rid of the unconjugated hairpins, the mixture solutions were centrifuged (15,000 rpm, 20 min) and then collected. The collected DNA-WP was washed three times by centrifugation (15,000 rpm, 15 min), resuspended in PBS (600 μL), and stored at 4 °C until use.

Fluorescence Measurements. Telomerase/mup53 extracts (10 μL), 5 μL of $ZnCl_2/MgCl_2$ solution (20 mM), and 100 μL of DNA-WP (part 1 or part 2) were mixed and incubated for 1 h; then, the reaction products of the method were directly measured by the fluorescence spectrophotometer. The excitation wavelength was set at 530 nm for mup53 detection and 480 nm for telomerase detection. Before each measurement, the quartz fluorescence cell was rinsed three times in 70% ethanol and another three times in distilled water.

Gel Electrophoresis Analysis. The gel was prepared in 1× Tris-borate-EDTA buffer. The agarose gel was first run in 1× Tris-borate-EDTA buffer at 70 V for 45 min and then stained by ethidium bromide. Finally, the gel was imaged using a Bio-Rad molecular imager under blue light.

Preparation of Fuel Sequence-Encapsulated Liposomes. The fuel sequence (2 μL, 100 μM) was mixed with 20 μL of serum-free medium, while 1.0 μL of Lipo-2000 was dissolved in 20 μL of serum-free medium and incubated for 10 min at room temperature. After the two solutions were mixed and incubated for 30 min at room temperature, fuel sequence-encapsulated liposomes were obtained.

Confocal Fluorescence Imaging. The cells were cultured in a confocal dish containing serum medium until they were attached to the bottom of the dish. Next, 200 μL of DNA-WP was added and incubated for 4 h. Then, 2 μL of 100 μM fuel sequence (wrapped into liposomes) was added to the confocal dish to mix with the cells and incubated for 2 h. Thereafter, the 200 μM Zn^{2+} was incubated with the cells for 30 min. Finally, the cells were washed with PBS solution three times. The treated cells were observed with 60× objective lenses to investigate the intracellular fluorescence distribution and intensity under the laser scanning confocal microscope.

Determination of Cell Viability. CCK-8 assays were carried out to evaluate the potential cytotoxicity of nanomachines toward HeLa cell lines. HeLa cells (1×10^4 cells mL^{-1}) were seeded in 96-well plates in DMEM culture medium in a humidified atmosphere containing 5% CO_2 at 37 °C for 12 h to make sure that the cells were completely adhered. Subsequently, different addition volumes and incubation times of DNA-WP were tested. Afterward, 10 μL of CCK-8 was added to each well, and the incubation was

https://doi.org/10.1021/acs.analchem.2c05111
Anal. Chem. 2023, 95, 4122−4130

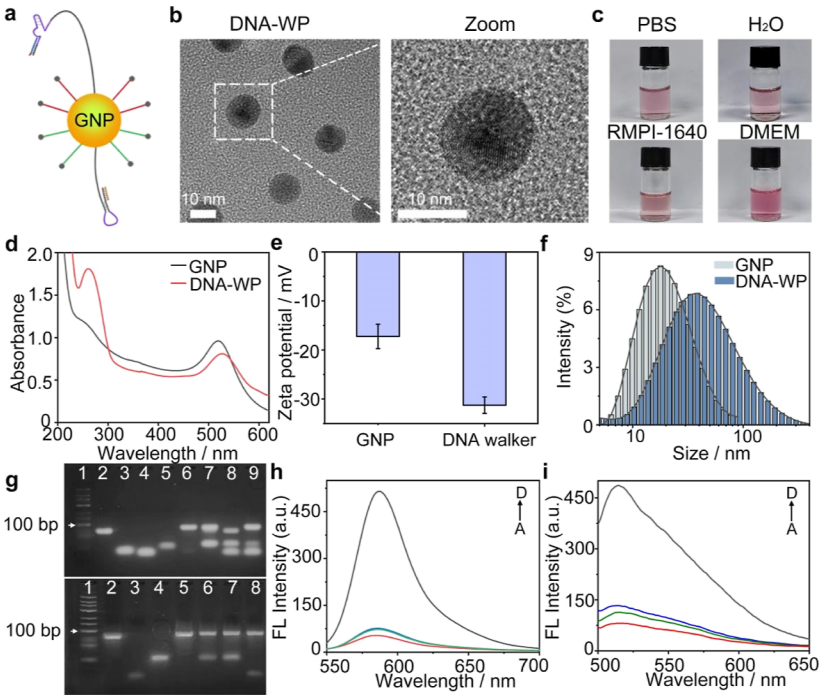

Figure 2. Fabrication and characterization of the DNA-WP. (a) DNA-WP structure (not in a real scale). (b) TEM images of DNA-WP. (c) Photographs of tubes containing the DNA-WP in PBS, H_2O, RMPI-1640, and DMEM. (d) UV−visible spectra, (e) ζ potentials, and (f) size distributions of GNPs before and after DNA modification. (g) Gel electrophoretic analysis of DNAzyme-controlled substrate cleavage. Top: ladder (lane 1), walking strand-1 (lane 2), protecting sequence (lane 3), fuel sequence (lane 4), substrate-1 (lane 5), mixture of walking strand-1 and protecting sequence (lane 6), mixture of walking strand-1, protecting sequence, fuel sequence and substrate-1 treated with mup53 (lane 7), mixture of walking strand-1, protecting sequence, fuel sequence, and substrate-1 treated with mup53 and Zn^{2+} (lane 8), and mixture of walking strand-1, protecting sequence, fuel sequence, and substrate-1 treated with wtp53 and Zn^{2+} (lane 9). Bottom: ladder (lane 1), walking strand-2 (lane 2), TSP (lane 3), substrate-2 (lane 4), mixture of walking strand-2 and TSP (lane 5), mixture of walking strand-2, TSP, and substrate-2 (lane 6), mixture of walking strand-2, TSP, and substrate-2 treated with Mg^{2+} (lane 7), and mixture of walking strand-2, TSP, and substrate-2 treated with telomerase and Mg^{2+} (lane 8). (h) Fluorescence spectra of the (A) DNA-WP, (B) DNA-WP + Zn^{2+}, (C) DNA-WP + fuel sequence + wtp53 + Zn^{2+}, and (D) DNA-WP + fuel sequence + mup53 + Zn^{2+}. (i) Fluorescence spectra of the (A) DNA-WP, (B) DNA-WP + Mg^{2+}, (C) DNA-WP + denatured telomerase + Mg^{2+}, and (D) DNA-WP + telomerase + Mg^{2+}.

continued in the incubator for 1.5 h. A microplate reader was used to detect the optical density (OD) value of CCK-8 at 450 nm.

RESULTS AND DISCUSSION

Design of the DNAzyme-Powered DNA Walker for Evaluation of p53 Mutation and Telomerase Activity. The designed DNA-WP consists of two function modules: the p53 mutation detection module (part 1) and the telomerase activity detection module (part 2). To evaluate intracellular p53 mutation, a walking strand containing a Zn^{2+}-specific DNAzyme sequence in the middle (walking strand-1) is attached on the GNP, and its 3′-end is locked with a protecting sequence to form a consensus double strand specifically recognizable to wild-type p53 (Figure S3). When no mutation exists (in normal cells), the walking strand is firmly locked by wild-type p53. When p53 mutation occurs in cancer cells, the linkage between the consensus double strand and p53 cannot happen, leading to unlocking of the walking strand by a fuel sequence and subsequent cleavage of the substrates by the activated DNAzyme to light up the fluorescence of Cy5. The fluorescence intensity is positively correlated with the mutation of p53 in cancer cells (Figure 1, part 1). For the analysis of telomerase activity, a walking strand containing a Mg^{2+}-specific DNAzyme sequence in the middle (walking strand-2) is assembled on the GNP, and its 3′-end generation is locked by a loop-stem structure (Figure S4). A TSP is hybridized with the walking stand to form an elongated stem structure with a nick in the middle. In the presence of telomerase, the TSP can be extended to generate repeated telomeric sequences, leading to substitutional hybridization to open the locked loop, thus allowing the reactivation of the DNAzyme. The subsequent substrate cleavage leads to the fluorescence recovery of FAM. The fluorescence intensity is positively related to the telomerase activity (Figure 1, part 2). By incubating the DNA-WP with living cells, the p53 mutation and telomerase activation can be visualized simultaneously by fluorescence imaging.

For the fabrication of the DNA-WP (Figure 2a), the ∼15 nm GNP cores were first synthesized with a classical citrate reduction method.[39] The locked walking strands and substrate strands were then modified on the surface of GNPs via Au−S linkage. As shown in the TEM image (Figure 2b and Figure S5) and photographs of the synthesized probe solution (Figure 2c), the GNPs were spherical and uniformly distributed without obvious aggregation. Using the DTT displacement method,[40] the amounts of substrate-1 and substrate-2 attached on the surface of GNPs were determined to be 100 per GNP and 96 per GNP, respectively. The numbers of DNAzyme sequence-1 and DNAzyme sequence-2 attached on the surface of GNPs were determined to be 10 per GNP and 10 per GNP, respectively (Figure S6). From the UV−vis absorption spectra

https://doi.org/10.1021/acs.analchem.2c05111
Anal. Chem. 2023, 95, 4122−4130

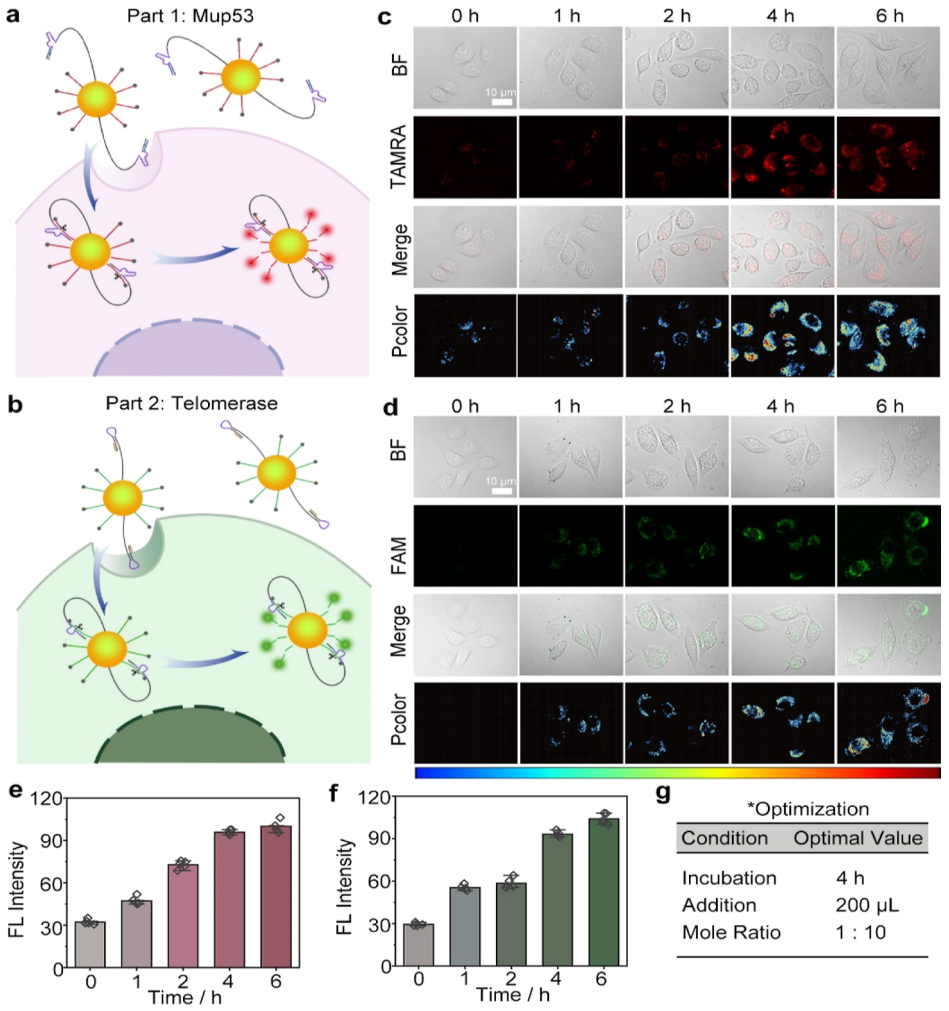

Figure 3. Optimization of reaction conditions for imaging of mup53 and telomerase in HeLa cells. (a,b) Schematic illustration of fluorescence imaging of (a) mup53 and (b) telomerase. (c,d) Confocal images of (c) mup53 and (d) telomerase in HeLa cells after different incubation times with the DNA-WP (200 μL) and then treatment with the corresponding metal ions (Zn^{2+} for mup53 and Mg^{2+} for telomerase) for 30 min. (e,f) FL intensity histogram of TAMRA in (c) and FAM in (d). (g) Optimized conditions for the imaging of mup53 and telomerase in HeLa cells. BF: bight field. Pcolor: pseudo-color of red or green channels; color bar: 35 to 250 from left to right.

(Figure 2d), the DNA-WP showed a characteristic peak of DNA structures at ~250 nm and a typical AuNP peak at 521 nm with a tiny red shift, indicating successful DNA modification. The ζ potential analysis (Figure 2e) and DLS characterization (Figure 2f) also confirmed the successful synthesis of the DNA-WP with increasing hydrodynamic diameter of the DNA-WP and more negative ζ potential compared with the bare GNP. To evaluate the target-propelled DNA walking, a gel electrophoresis experiment was conducted to characterize the cleavage of the substrate strands in the presence of mup53 or telomerase (Figure 2g). Owing to the fact that the protecting sequence and fuel sequence were completely matched, the walking strand-1 was activated (only locked by wild-type p53) to achieve the hybridization between DNAzyme sequence-1 and substrate-1 (lane 7). After adding the Zn^{2+} ion, the substrate-1 was cut at the ribonucleotide cleavage site (lane 8). In contrast, the combination of the protecting sequence and fuel sequence did not occur in the presence of wild-type p53; thus, the substrate-1 was not cleaved after the addition of zinc ions (lane 9). Next, the gel electrophoretic analysis of the telomerase-controlled substrate cleavage confirmed the reactivation of the DNAzyme in walking strand-2 triggered by telomerase, while the cleavage of substrate-2 was achieved after adding Mg^{2+} ions (lane 8). In contrast, the locked walking strand-2 could not be activated in the absence of telomerase, and substrate-2 did not change after the addition of Mg^{2+} ions (lane 6).

We then examined the feasibility of the DNA-WP for detecting mup53 and telomerase in aqueous solution (Figure 2h,i). In the absence of analytes, no obvious fluorescence was observed, suggesting effective fluorescence quenching by GNP cores. After the addition of the cofactor metal ion, the DNA-WP did not show the fluorescence response, as the DNAzymes were still blocked without analyte activation. In contrast, in the presence of mup53 (or telomerase), the walking strands were activated to cleave the substrate strands, and obvious increases in fluorescent intensities were observed (TAMRA and FAM, corresponding to mup53 and telomerase, respectively). These results confirmed the capability of the DNA-WP for the monitoring of mup53 and telomerase. We also evaluated the stability of the prepared DNA-WP in H_2O, PBS, DMEM, and RPMI-1640. After the 24 h observation period, the DNA-WP did not exhibit turbidity, precipitation, or color change in the

https://doi.org/10.1021/acs.analchem.2c05111
Anal. Chem. 2023, 95, 4122−4130

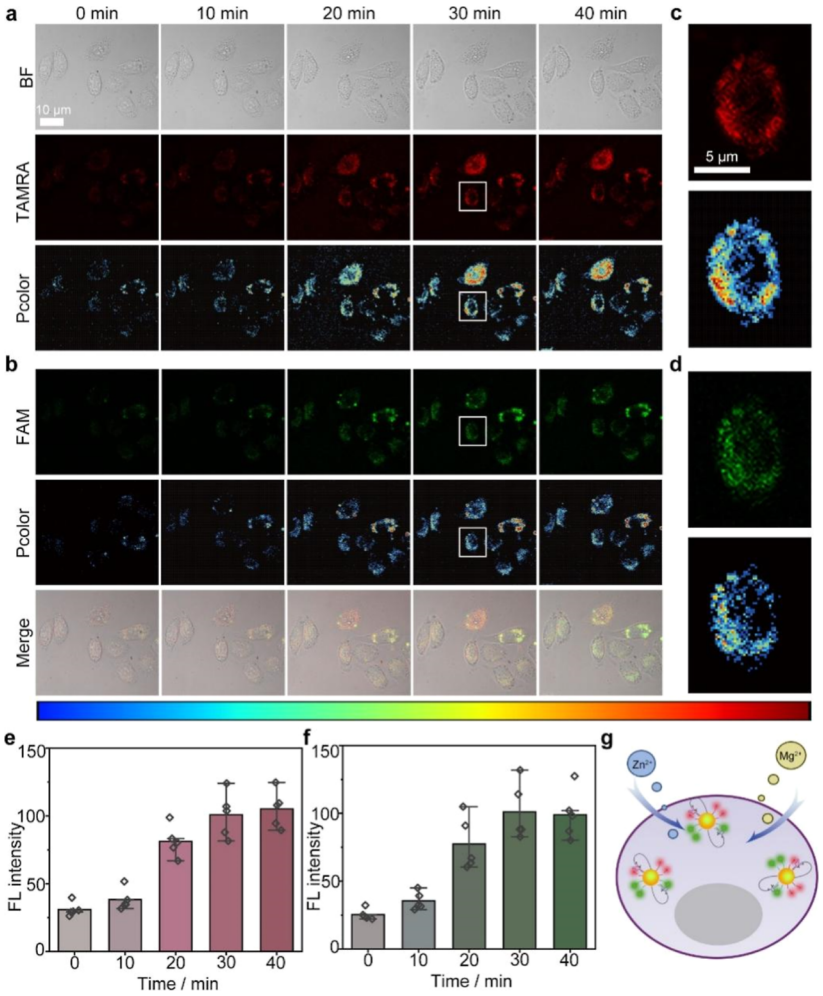

Figure 4. Confocal imaging of mup53 and telomerase in HeLa cells with the DNA-WP strategy. (a,b) Confocal images of (a) mup53 and (b) telomerase in DNA-WP-treated HeLa cells after incubation with 200 μM Zn^{2+} or Mg^{2+} for different times. (c,d) Enlarged images and pseudo-color maps of a single HeLa cell selected from (a) and (b). (e,f) FL intensity histogram of TAMRA in (a) and FAM in (b). (g) Schematic illustration of the simultaneous intracellular imaging principle of mup53 and telomerase with the DNA-WP under the supplement of Zn^{2+} and Mg^{2+}. BF: bight field, Pcolor: pseudo-color of red or green channel intensity; color bar: 35 to 250 from left to right.

four tested media (Figure S7). These results demonstrated the good dispersity and stability of the DNA-WP.

Visualization of p53 Mutation and Telomerase Activity in Cancer Cells. Before cell experiments, the cytotoxicity of the DNA-WP was investigated. After incubating HeLa cells with the DNA-WP at different addition volumes for different incubation times, the viability of the cells was maintained, indicating low cytotoxicity of the probe (Figure S8). To verify the feasibility of the nanoprobe for in situ imaging, HeLa cells were sequentially incubated with the DNA-WP, fuel sequence, and metal ions. The confocal images did not show the fluorescence signal in the absence of metal ions (Figure S9), which confirmed the stability of substrate strands on AuNPs. In addition, the DNAzyme walking strands could not also be activated in the absence of fuel sequences or primer elongation, as observed from the neglectable fluorescence (Figure S10). Only when the DNA-WP, fuel sequence, and metal ions coexisted, bright red and green fluorescence was detected in HeLa cells, which confirmed that the DNA-WP operated successfully in living cells. Therefore, the DNAzyme-powered DNA walker amplification strategy allows to image dual mup53 and telomerase in living cells.

To obtain the best confocal fluorescence images, the reaction conditions including the incubation time, the additional volume of the DNA-WP, and the mole ratio of the walking strands to the substrate strands were optimized by testing the orthogonal fluorescence recovery of mup53 and telomerase separately. As shown in Figure 3a–d, the fluorescence of mup53 (TAMRA) and telomerase (FAM) in HeLa cells gradually increased with the increasing incubation time and then reached a plateau after 4 h. Corresponding fluorescence intensity histograms further confirmed the abovementioned results (Figure 3e,f). Thus, an optimized incubation time of 4 h was used for the following cell experiments. Similarly, the additional volume of the DNA-WP was optimized to be 200 μL (Figure S11).

To maximize the fluorescence signal, a series of DNA-WPs were synthesized with different walking strand/substrate strand ratios of 1:2, 1:5, 1:10, and 1:20 for assessing the signal amplification effect. The fluorescence recovery triggered by analytes was tested. During the observation period of 4 h, the fluorescence recovery of the DNA-WP with a walking strand/substrate strand ratio of 1:10 was the highest (Figure S12); thus, a mole ratio of 1:10 was used in the subsequent experiments. The optimized conditions for the imaging of

https://doi.org/10.1021/acs.analchem.2c05111
Anal. Chem. 2023, 95, 4122−4130

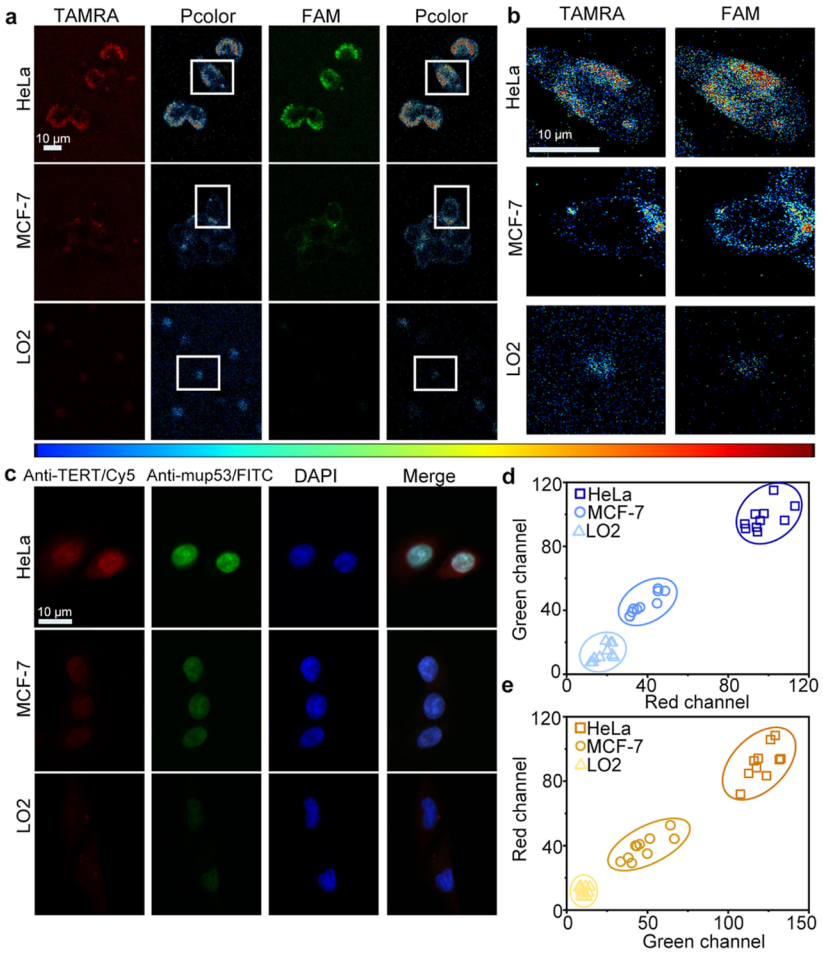

Figure 5. Confocal imaging of mup53 and telomerase in different cell lines. (a) Confocal imaging of mup53 (TAMRA) and activated telomerase (FAM) with the DNA-WP strategy. (b) Enlarged pseudo-color maps of single cells selected from (a) in the white squares. (c) Microscopy imaging of mup53 and telomerase in cell lines by immunostaining with anti-TERT/Cy5 (red) and anti-p53/FITC (green). (d) Fluorescence distribution of mup53 (TAMRA)/telomerase (FAM) corresponding to DNA-WP-treated cells in (a). (e) Fluorescence distribution of anti-mup53 (FITC)/anti-TERT (Cy5) corresponding to immunostained cells in (c). A total of 10 cells for each cell type. Merge: mixed green and red channels, and mixed green, red, and blue channels. Color bar: 35 to 250 from left to right.

mup53 and telomerase in HeLa cells were 4 h incubation, 200 μL (addition volume), and 1:10 mole ratio (Figure 3g).

Under the optimal reaction conditions, the ability of the DNA-WP to image dual mup53 and telomerase simultaneously in HeLa cells upon the treatment with metal ions was tested. As shown in Figure 4a–d, the red and green fluorescence in the cells became brighter as the treatment times of metal ions increased from 0 to 30 min. The corresponding fluorescence intensity also confirmed the abovementioned results (Figure 4e,f). The simultaneous intracellular imaging principle of mup53 and telomerase by the DNA-WP is illustrated in Figure 4g.

Comparison of p53 Mutation and Telomerase Activity in Different Cell Lines. Since mup53 and telomerase are considered as cancer biomarkers with upregulated expression in cancer cells, we investigated the adaptability of the DNA-WP method for monitoring of mup53 and telomerase in HeLa cells, MCF-7 cells, and LO2 normal cells. As shown in Figure 5a, the fluorescence signals in cancer cells (HeLa cells and MCF-7 cells) were significantly higher than those in normal cells (LO2 cells). The expression levels of telomerase were distinguishable in the three cell lines as follows: HeLa > MCF-7 > LO2, which was in accordance with the expression levels of mup53. By checking the enlarged pseudo-color maps of the nanoprobes in single cells (Figure 5b), we found that the average red and green channel intensity decreased from HeLa to LO2 cells, which confirmed the abovementioned results. To verify the expression difference of mup53 and telomerase in different cell lines, we next examined the cellular distribution of mup53 and telomerase by immunofluorescent (IF) staining. The fluorescence images of anti-mup53/FITC and anti-TERT/Cy5 (associated with telomerase) revealed that mup53 and telomerase levels in HeLa cells were relatively higher than in MCF-7 cells, while the mup53 and telomerase in LO2 cells were neglectable (Figure 5c), which was consistent with the abovementioned experiments with the proposed DNA-WP. Cancer cells (HeLa cells and MCF-7 cells) could be easily discriminated from normal cells (LO2) with the fluorescence distribution (Figure 5d,e), which indicated the great potential of the DNA walker-based strategy for cancer diagnosis.

Cooperative Expression of Mutant p53 and Telomerase under Drug Treatment. Considering the good imaging performance of the DNA-WP in living cells, the DNA-WP-based dual imaging protocol was used for monitoring the cooperative expression of mup53 and telomerase upon the

https://doi.org/10.1021/acs.analchem.2c05111
Anal. Chem. 2023, 95, 4122−4130

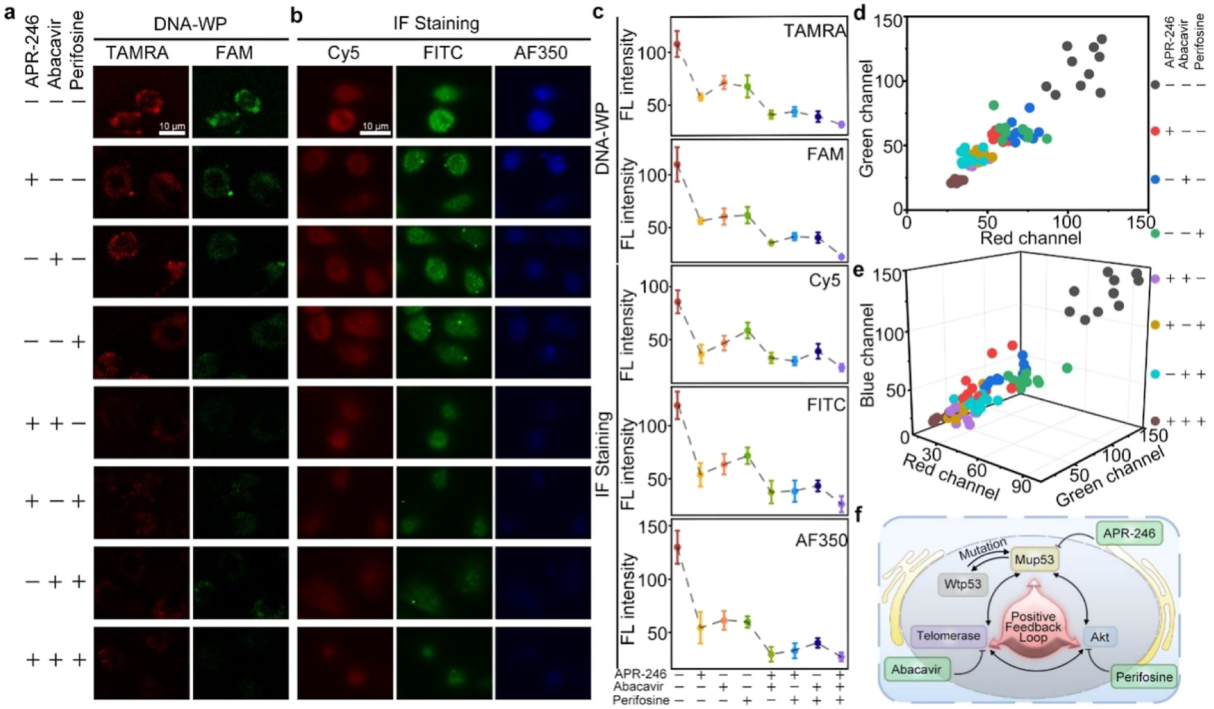

Figure 6. Correlation of mup53 and telomerase with the Akt pathway under different drug treatments. (a) Confocal images of HeLa cells treated with different drugs for 24 h and then imaged with the DNA-WP strategy. (b) Confocal imaging of the expression levels of mup53 and telomerase and Akt in HeLa cells treated with different drugs for 24 h and then immunostained by anti-p53/FITC (green), anti-TERT/Cy5 (red), and anti-Akt/AF350 (blue). (c) FL intensity comparison of TAMRA, FAM, Cy5, FITC, and AF350 in (a) and (b). Each point in the plots represents a condition of drug treatment. From left to right: control, APR246, abacavir, perifosine, APR246 and abacavir, APR246 and perifosine, abacavir and perifosine, APR246, abacavir, and perifosine. (d) fluorescence distribution of mup53 (TAMRA)/telomerase (FAM) corresponding to DNA-WP-treated cells under different drug treatments in (a). (e) Fluorescence distribution of anti-TERT (Cy5)/anti-mup53 (FITC)/anti-Akt (AF350) corresponding to immunostained cells under different drug treatments in (b). (f) Schematic illustration showing the networks between mup53, telomerase, and Akt in cancer cells.

treatment of various antitumor drugs. To explore the delicate networks between mup53 and telomerase, different combinations of drugs including APR-246 (mup53 inhibitor), abacavir (telomerase inhibitor), and perifosine (Akt inhibitor) were used to treat HeLa cells. The obvious inhibition of mup53 and telomerase induced by APR-246, abacavir, and perifosine was observed (Figure 6a), suggesting an intrinsic connection of mup53, telomerase, and Akt. Furthermore, the multiple application of these drugs induced higher downregulation of mup53 and telomerase. Consistently, the highest downregulation was achieved by the combination of all three drugs. Next, the expression changes of mup53, telomerase, and Akt under different drug treatments were further examined by immunofluorescence imaging (Figure 6b), and the obtained results were consistent with the data obtained by using the DNA-WP strategy. The FL intensity comparison of FAM, TAMRA, FITC, Cy5, and AF350 indicated obvious expression changes in mup53 and telomerase after drug treatments (Figure 6c). From the scatter plots showing the fluorescence distribution (Figure 6d,e), the cells could be obviously divided into eight different zones under different drug treatments. These results suggested a significant intrinsic correlation between the expression of mup53 and telomerase and Akt pathway (Figure S13). It is worth noting that a positive feedback loop between mup53, telomerase, and the Akt pathway was demonstrated in cancer cells (Figure 6f), which was important for understanding the complex networks between cancer biomarkers and cellular pathways.

CONCLUSIONS

A DNAzyme-powered DNA walker has been developed as a nanoprobe for the imaging of cooperative expression of mup53 and telomerase in living cells. This nanoprobe can be activated after specific recognition of mup53 and telomerase in an orthogonal manner, as the DNAzyme walking strands can continuously and automatically cleave corresponding substrates assembled on the nanoprobe surface in the presence of metal ions, thus eventually producing a large number of fluorescent fragments. We have demonstrated the successful use of the DNA walker nanoprobe for the real-time multiplex visualization of the mup53 and telomerase in living cells and applied the proposed protocol for investigating the expression changes in the two biomarkers under the treatment of different antitumor drugs. Furthermore, we discovered that mup53 and telomerase could be cooperatively activated in cancer cells via the Akt pathway, which may potentially contribute to the guidance of cancer treatment options.

ASSOCIATED CONTENT

Supporting Information

The Supporting Information is available free of charge at https://pubs.acs.org/doi/10.1021/acs.analchem.2c05111.

Details on experimental methods, images used for analysis, control experiments, and additional examples (PDF)

https://doi.org/10.1021/acs.analchem.2c05111
Anal. Chem. 2023, 95, 4122−4130

AUTHOR INFORMATION

Corresponding Authors

Ruo-Can Qian − *Key Laboratory for Advanced Materials, Feringa Nobel Prize Scientist Joint Research Center, Joint International Laboratory for Precision Chemistry, Frontiers Science Center for Materiobiology & Dynamic Chemistry, School of Chemistry and Molecular Engineering, East China University of Science and Technology, Shanghai 200237, P. R. China;* orcid.org/0000-0002-1039-9866; Email: ruocanqian@ecust.edu.cn

Huangxian Ju − *State Key Laboratory of Analytical Chemistry for Life Science, School of Chemistry and Chemical Engineering, Nanjing University, Nanjing 210023, P. R. China;* orcid.org/0000-0002-6741-5302; Email: hxju@nju.edu.cn

Authors

Ze-Rui Zhou − *Key Laboratory for Advanced Materials, Feringa Nobel Prize Scientist Joint Research Center, Joint International Laboratory for Precision Chemistry, Frontiers Science Center for Materiobiology & Dynamic Chemistry, School of Chemistry and Molecular Engineering, East China University of Science and Technology, Shanghai 200237, P. R. China;* orcid.org/0000-0001-9089-8480

Da-Wei Li − *Key Laboratory for Advanced Materials, Feringa Nobel Prize Scientist Joint Research Center, Joint International Laboratory for Precision Chemistry, Frontiers Science Center for Materiobiology & Dynamic Chemistry, School of Chemistry and Molecular Engineering, East China University of Science and Technology, Shanghai 200237, P. R. China;* orcid.org/0000-0002-9257-4452

Complete contact information is available at: https://pubs.acs.org/10.1021/acs.analchem.2c05111

Notes

The authors declare no competing financial interest.

ACKNOWLEDGMENTS

This research was supported by the National Natural Science Foundation of China (21977031 and 21890741), National Science and Technology Major Project of China (2018ZX10302205), and Fundamental Research Funds for the Central Universities. The authors thank Dr. Bo-Hao Yu at the Research Center of Analysis and Test of East China University of Science and Technology for help in laser scanning confocal microscopy analysis.

REFERENCES

(1) Deepa; Pundir, S.; Pundir, C. S. *Anal. Biochem.* **2020**, *588*, 113473.
(2) Kyo, S.; Takahura, M.; Inoue, M. *Histol. Histopathol.* **2000**, *15*, 813−824.
(3) Li, J.; Wang, J.; Liu, S.; Xie, N. K.; Quan, Y.; Yang, X.; Yang, J.; Huang, K.; Wang, K. *Angew. Chem., Int. Ed.* **2020**, *59*, 20104−20111.
(4) Vogelstein, B.; Lane, D.; Levine, A. J. *Nature* **2000**, *408*, 307−310.
(5) Kastenhuber, E. R.; Lowe, S. W. *Cell* **2017**, *170*, 1062−1078.
(6) El-Deiry, W. S.; Kern, S. E.; Pietenpol, J. A.; Kinzler, K. W.; Vogelstein, B. *Nat. Genet.* **1992**, *1*, 45−49.
(7) Hafner, A.; Bulyk, M. L.; Jambhekar, A.; Lahav, G. *Nat. Rev. Mol. Cell Biol.* **2019**, *20*, 199−210.
(8) Goh, A. M.; Coffill, C. R.; Lane, D. P. *J. Pathol.* **2010**, *223*, 116−126.
(9) Oren, M.; Rotter, V. *Cold Spring Harb. Perspect. Biol.* **2010**, *2*, a001107.
(10) Rudolph, K. L.; Chang, S.; Lee, H. W.; Blasco, M.; Gottlieb, G. J.; Greider, C.; DePinho, R. A. *Cell* **1999**, *96*, 701.
(11) Shay, J. W.; Bacchetti, S. A.; Shay, J. W.; Bacchetti, S. *Eur. J. Cancer* **1997**, *33*, 787−791.
(12) Blackburn, E. H. *Annu. Rev. Biochem.* **1992**, *61*, 113−129.
(13) Harley, C. B. *Nat. Rev. Cancer* **2008**, *8*, 167−179.
(14) Gould, K. A.; Nixon, C.; Tilby, M. J. *Mol. Pharmacol.* **2004**, *66*, 1301−1309.
(15) Gaballah, E. T. M. A.; Tawfik, M. A. *Saudi Dent J .* **2010**, *22*, 167−170.
(16) Attallah, A. M.; Abdel-Aziz, M. M.; El-Sayed, A. M.; Tabll, A. A. *Cancer Detect. Prev.* **2003**, *27*, 127−131.
(17) Benchimol, S.; Pim, D.; Crawford, L. *EMBO J.* **1982**, *1*, 1055−1062.
(18) Emrich, T.; Karl, G. *Methods Mol. Biol.* **2002**, *191*, 147−158.
(19) Liu, D. *Int. J. Electrochem. Sci.* **2020**, *15*, 11371−11386.
(20) Pedrero, M.; Manuel de Villena, F. J. M.; Muñoz-San Martín, C. M.-S.; Campuzano, S.; Garranzo-Asensio, M. G.; Barderas, R.; Pingarrón, J. M. *Biosensors* **2016**, *6*, 56.
(21) Wang, X.; Wang, Y.; Jiang, M.; Shan, Y.; Jin, X.; Gong, M.; Wang, X. *Anal. Biochem.* **2018**, *548*, 15−22.
(22) Afsharan, H.; Navaeipour, F.; Khalilzadeh, B.; Tajalli, H.; Mollabashi, M.; Ahar, M. J.; Rashidi, M.-R. *Biosens. Bioelectron.* **2016**, *80*, 146−153.
(23) Bizzarri, A. R.; Moscetti, I.; Cannistraro, S. *Anal. Chim. Acta* **2018**, *1029*, 86−96.
(24) Davis, A. P. *Nature* **1999**, *401*, 120−121.
(25) Kay, E. R.; Leigh, D. A. *Angew. Chem., Int. Ed.* **2015**, *54*, 10080−10088.
(26) Wang, W. J.; Yu, S.; Huang, S.; Bi, S.; Han, H. Y.; Zhang, J.-R.; Lu, Y.; Zhu, J.-J. *Chem. Soc. Rev.* **2019**, *48*, 4892−4920.
(27) Pan, J.; Li, F.; Cha, T.-G.; Chen, H.; Choi, J. H. *Curr. Opin. Biotechnol.* **2015**, *34*, 56−64.
(28) Shin, J.-S.; Pierce, N. A. *J. Am. Chem. Soc.* **2004**, *126*, 10834−10835.
(29) Sherman, W. B.; Seeman, N. C. *Nano Lett.* **2004**, *4*, 1203−1207.
(30) Yin, P.; Yan, H.; Daniell, X. G.; Turberfield, A. J.; Reif, J. H. *Angew. Chem., Int. Ed.* **2004**, *43*, 4906−4911.
(31) You, M.; Chen, Y.; Zhang, X.; Liu, H.; Wang, R.; Wang, K.; Williams, K. R.; Tan, W. *Angew. Chem., Int. Ed.* **2012**, *51*, 2457−2460.
(32) Yang, X.; Tang, Y.; Mason, S. D.; Chen, J.; Li, F. *ACS Nano* **2016**, *10*, 2324−2330.
(33) Zhang, H.; Xu, X.; Jiang, W. *Chem. Sci.* **2020**, *11*, 7415−7423.
(34) Li, J.; Wang, J.; Liu, S.; Xie, N.; Quan, K.; Yang, Y.; Yang, X.; Huang, J.; Wang, K. *Angew. Chem., Int. Ed.* **2020**, *132*, 20279−20286.
(35) Hwang, K.; Hosseinzadeh, P.; Lu, Y. *Inorg. Chim. Acta* **2016**, *452*, 12−24.
(36) Li, Y.; Breaker, R. R. *Curr. Opin. Struct. Biol.* **1999**, *9*, 315−323.
(37) Hwang, K.; Mou, Q.; Lake, R. J.; Xiong, M.; Holland, B.; Lu, Y. *Inorg. Chem.* **2019**, *58*, 13696−13708.
(38) Liu, J.; Lu, Y. *J. Am. Chem. Soc.* **2002**, *124*, 15208−15216.
(39) Nativo, P.; Prior, I. A.; Brust, M. *ACS Nano* **2008**, *2*, 1639−1644.
(40) Hurst, S. J.; Lytton-Jean, A. K. R.; Mirkin, C. A. *Anal. Chem.* **2006**, *78*, 8313−8318.